# Double-Wall Carbon Nanotubes for Wide-Band, Ultrafast Pulse Generation

**Tawfique Hasan,[†,*] Zhipei Sun,[‡] PingHeng Tan,[§] Daniel Popa,[†] Emmanuel Flahaut,[⊥,∥] Edmund J. R. Kelleher,[#] Francesco Bonaccorso,[¶,▲] Fengqiu Wang,[▽] Zhe Jiang,[†] Felice Torrisi,[†] Giulia Privitera,[†] Valeria Nicolosi,[■] and Andrea C. Ferrari[†]**

[†]Cambridge Graphene Centre, University of Cambridge, Cambridge CB3 0FA, United Kingdom, [‡]Department of Micro- and Nanosciences, Aalto University, FI-00076 Aalto, Finland, [§]State Key Laboratory for Superlattices and Microstructures, Beijing 100083, China, [⊥]Université de Toulouse; UPS, INP; Institut Carnot Cirimat; 118, route de Narbonne, F-31062 Toulouse cedex 9, France, [∥]CNRS; Institut Carnot Cirimat; F-31062 Toulouse, France, [#]Femtosecond Optics Group, Department of Physics, Imperial College, London SW7 2AZ, United Kingdom, [¶]CNR-Istituto Processi Chimico-Fisici, 98158 Messina, Italy, [▲]Istituto Italiano di Tecnologia, Graphene Labs, 16163, Genova, Italy, [▽]School of Electronic Science and Engineering, Nanjing University, Nanjing 210023, China, and [■]School of Chemistry, School of Physics, CRANN and AMBER, Trinity College Dublin D2, Ireland

**ABSTRACT** We demonstrate wide-band ultrafast optical pulse generation at 1, 1.5, and 2 $\mu$m using a single-polymer composite saturable absorber based on double-wall carbon nanotubes (DWNTs). The freestanding optical quality polymer composite is prepared from nanotubes dispersed in water with poly(vinyl alcohol) as the host matrix. The composite is then integrated into ytterbium-, erbium-, and thulium-doped fiber laser cavities. Using this single DWNT—polymer composite, we achieve 4.85 ps, 532 fs, and 1.6 ps mode-locked pulses at 1066, 1559, and 1883 nm, respectively, highlighting the potential of DWNTs for wide-band ultrafast photonics.

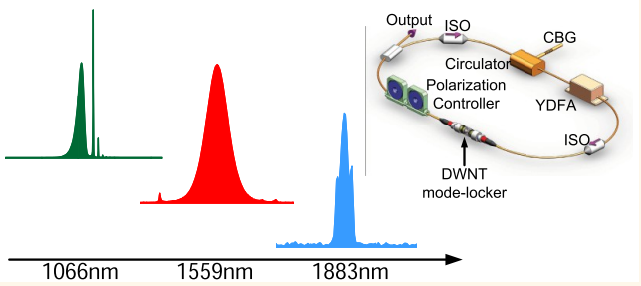


**KEYWORDS:** double-wall carbon nanotubes · polymer composites · saturable absorber · ultrafast laser

Materials with nonlinear optical properties are of critical importance for a diverse range of photonic applications,[1] such as optical regeneration,[2−4] switching,[2,5,6] modulation,[7,8] sampling,[9,10] and noise suppression.[11] In this field, one of the most sought-after applications involves generation of ultrafast laser pulses.[12,13] Indeed, laser sources producing nano- to sub-picosecond optical pulses are a major component in the product portfolio of leading laser manufacturers.[12] Many of the relevant applications, ranging from basic scientific research to materials processing, from eye surgery to printed circuit board manufacturing, from metrology to trimming of electronic components (*e.g.*, resistors and capacitors) currently employ laser sources utilizing a mode-locking technique based on a nonlinear optical material, called saturable absorber (SA). These SAs, when placed in a laser cavity, modify the laser continuous-wave output into a train of ultrashort optical pulses.[12] The key requirements for such nonlinear optical materials are fast response time, large nonlinearity, broad wavelength range, low optical loss, high power handling, low cost, and ease of integration into an optical system.[12] Currently, the dominant commercial SA technology is based on semiconductor saturable absorber mirrors (SESAMs).[14] However, these typically have limited operation bandwidths (a few tens of nanometers[12,13]) and require complex fabrication and packaging.[12] A simpler and cost-effective alternative relies on using single-wall carbon nanotubes (SWNTs)[15−28] or graphene.[15,28−40] While wide-band operation in SWNT-based devices can be achieved using a distribution of tube diameters,[15,21,28,41,42] this is an intrinsic property of graphene, due to the gapless linear dispersion of Dirac electrons.[31,42,43]

In general, a good SA should have a high (*e.g.*, ∼10% for fiber lasers[13]) modulation depth (the absorption change between high and low intensity optical irradiation).[12,42] However, for a pristine single-layer graphene device, the optical absorption is relatively

* Address correspondence to th270@cam.ac.uk.

Received for review February 7, 2014 and accepted April 15, 2014.

**Published online April 15, 2014**
**10.1021/nn500767b**

low (~2.3%), making it unsuitable for fiber lasers where large optical absorption and modulation depth are typically needed.[13] For a given optical absorption, high modulation depth can be typically achieved by minimizing the nonsaturable losses (the optical loss of SAs at high irradiation intensity).[44] For SWNT-based SAs, nanotube bundles and aggregations mostly contribute to these. The most widely employed approach to avoid excessive nonsaturable losses is debundling the SWNTs *via* solution processing techniques and embedding them into polymer matrices.[42] Indeed, this strategy, coupled with matching the SWNT absorption peak with the operation wavelength, is followed in the majority of the SWNT-based photonic devices,[15,36,42] giving a typical nonsaturable loss of ~50% of total linear absorption.[15,42] However, when using a wide range of tube diameters to achieve a "wide-band" SWNT SA, the high loading of SWNTs required in the devices results in instability of nanotube dispersion during the composite preparation, leading to aggregation and, therefore, high nonsaturable absorption losses and small modulation depth.

Good SAs should also have a low value of saturation intensity,[45] $I_{sat}$. This is defined as the optical intensity required to reduce the SA absorption coefficient to half of the initial value, considering zero nonsaturable absorption losses.[44] In graphene, $I_{sat}$ is estimated to be in the range of a few tens[30,46,47] of MW/cm$^2$. For SWNTs, $I_{sat}$ is in the range of ~30 GW/cm$^2$ in aqueous dispersions.[48] For multiwall nanotubes (MWNTs) with ~40 nm outer diameter, $I_{sat}$ is >100 GW/cm$^2$ in aqueous dispersions.[49,50] Therefore, when compared with SWNTs and graphene, MWNTs require higher irradiation intensity to reach absorption saturation.[49,50] This is why, except for only a handful of reports,[51] MWNTs have not been traditionally considered as SAs for passive mode-locking.

The concentric tube arrangement makes DWNTs an interesting class of nanomaterials, with wide-ranging potential applications, including in (opto)electronics.[52−54] Of particular interest relevant to this work, DWNTs also exhibit ultrafast carrier dynamics.[48,55−57] Kamaraju *et al.*[48] measured a linear limit of saturable absorption ($\alpha_0 \sim 6.1 \times 10^3$ and $\sim 6.4 \times 10^3$ cm$^{-1}$) and $I_{sat}$ (~68 and 14 GW/cm$^2$) for aqueous dispersions and thin films of DWNTs, respectively. This is similar to the values reported for SWNT aqueous dispersions by the same authors ($\alpha_0 \sim 5.6 \times 10^4$ cm$^{-1}$ and $I_{sat} \sim 33$ GW/cm$^2$, respectively).[48] Thus, in terms of carrier dynamics, DWNTs are comparable to SWNTs.

Further, DWNTs can have outer and inner wall combinations with different electronic types (semiconducting, *s*, or metallic, *m*) in their structures (outer-inner: *s-s*, *s-m*, *m-s*, and *m-m*), resulting in different charge transfer behaviors between the tubes.[58] With a semiconducting outer tube for *s-s* and *s-m* combinations, optical absorption from excitonic transition energies of both the inner and outer walls is expected to contribute to the overall optical absorption of the resultant DWNT structure, making them suitable as wide-band SAs. Conversely, with metallic outer wall for the *m-s* and *m-m* combinations, the outer wall has zero band gap with wide absorption range and may create a screening effect,[59] suppressing optical absorption from the inner *s*- or *m*-nanotubes. Nevertheless, such combination may also work as an advantage for ultrafast photonic applications of DWNTs. This is because the presence of inner or outer *m*-nanotubes (*s-m*, *m-s*) in the same structure can increase the carrier relaxation speed of the *s*-nanotubes as electrons and holes can tunnel from them to their metallic counterparts.[60,61] Indeed, experimental observations indicate that the relaxation times of inner nanotubes of DWNTs are comparable or shorter[60,62,63] than the SWNTs of same species. For example, Nakamura *et al.*[57] showed that, under the same experimental conditions, the exciton decay time for (7,6) inner tubes in DWNTs is 0.65 ps, compared to 3.2 ps for a (7,6) SWNT species due to shorter exciton decay time and energy relaxation from inner to outer tubes[57] *via* exciton energy transfer (EET).[64,65]

The strong third-order optical nonlinearity, ultrafast carrier dynamics,[48,55−57,63] and wide optical absorption[57,66] make DWNTs with ~1.6−1.8 nm outer diameter very attractive for ultrafast photonic applications in the 1 to 2 $\mu$m range. With an interwall distance of ~0.36−0.38 nm,[67,68] the diameter difference between inner and outer tubes is ~0.7−0.8 nm. Therefore, DWNTs with 0.8−1.1 nm inner diameter have outer tubes with 1.6−1.8 nm diameter with two distinct and strong $eh_{22}$ and $eh_{11}$ *s*-tube absorption bands at ~1.1 and ~2.0 $\mu$m,[69] respectively. The $eh_{11}$ from inner *s*-tubes at ~0.8−1.1 $\mu$m are expected to be overlapped by $eh_{22}$ of the outer tubes.[66,69] This makes DWNTs efficient SAs at ~1 and ~2 $\mu$m and for larger diameter tubes, potentially beyond this range. This is very attractive for biomedical and biosensing applications where significant demand exists for portable, tunable, pulsed laser sources from ~2 to up to 10 $\mu$m.[70]

Similar to other nanoparticles, the aggregation phenomenon of nanotubes, especially in low viscosity dispersions, is largely governed by the diffusion process of nanotubes and nanotube−nanotube interactions in a certain medium.[71] This is in addition to the effect of solvent properties (*e.g.*, pH) and stabilization by dispersant (*e.g.*, surfactants). In low viscosity dispersions, aggregation between nanotubes can therefore increase significantly with increased nanotube concentration because of more "exposed" nanotube surfaces.[72] The processing technique we use here involves slow evaporation of solvents from a low viscosity (1.6 mPa·s at 25 °C) mixture. This highlights the need for a stable dispersion to avoid large aggregation during solvent evaporation. DWNTs allow two

nanotubes in a single structure, minimizing the possibility of such large (>1 $\mu$m) aggregations and bundle formation during composite fabrication and thus scattering losses while potentially offering high modulation depth at a range of wavelengths. Thus, they are potentially an attractive class of carbon nanomaterial for wide-band ultrafast pulse generation. Here, we demonstrate DWNT–polymer composites as wide-band passive mode-lockers for ultrafast pulse generation at 1, 1.5, and 2 $\mu$m in Yb-, Er-, and Tm-doped fiber laser cavities, respectively.

## RESULTS AND DISCUSSION

We use DWNTs produced by catalytic chemical vapor deposition (CCVD) of $CH_4$ over $Mg_{1-x}Co_xO$ solid solution containing Mo oxide.[73] After CCVD, the nanotubes are oxidized in air at 570 °C for 30 min.[74] The residual material is next washed with HCl to dissolve the metal oxides.[74] Figure 1a–c shows representative transmission electron microscopy (TEM) images of the DWNT samples at different magnifications. Statistics on ~130 DWNTs reveal that they have ~1.1 nm inner and ~1.8 nm outer mean diameters (Figure 1d,e). TEM images of ~145 tubes also indicate that the purified samples contain ~90% DWNTs, ~8% SWNTs, and ~2% triple-wall carbon nanotubes (TWNTs).

Optical absorption and photoluminescence excitation (PLE) spectroscopy of this purified nanotube sample dispersed with sodium dodecylbenzenesulfonate (SDBS) surfactant in deuterium oxide ($D_2O$) is then used to characterize the DWNT samples. Using $D_2O$ instead of water allows extension of the spectral study region of the dispersions in the NIR. Pure water begins to absorb at ~700 nm, followed by a series of strong absorption peaks above ~900 nm, with complete absorption just above 1100 nm. Using $D_2O$ instead of $H_2O$ means O–H is substituted by O–D, pushing all these water-related absorption peaks by ~$\sqrt{2}$ times toward the higher wavelength, that is, to beyond ~1300 and ~1800 nm for the case of the strong peaks and complete absorption, respectively.

Figure 2 plots the absorption spectrum of the purified nanotubes dispersed in $D_2O$. The peak at ~1.1 $\mu$m corresponds to $eh_{11}$ excitonic transitions of 0.75–1.15 nm inner tubes, overlapping with the $eh_{22}$ of 1.5–1.9 nm outer tubes.[66,69] The reference spectrum of $D_2O$ is also presented, highlighting that the $eh_{22}$ absorption peaks of the outer wall of DWNTs cannot be resolved above 1800 nm due to strong optical absorption from $D_2O$.

Figure 3 plots the PLE map of the purified nanotube sample (~90% DWNTs, ~8% SWNTs, and ~2% TWNTs). The chiralities are assigned according to ref 69. The PLE map shows strong emissions from the diameter range of ~0.7–1.15 nm. This corresponds to that of the inner tubes as derived by TEM (Figure 1e). Tan *et al.*[64,65] reported ~2–3 meV red-shift in $eh_{11}$ and $eh_{22}$ of small

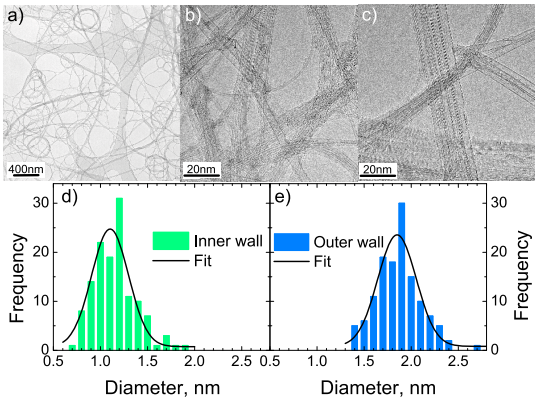


**Figure 1. (a–c) Representative TEM images of the purified DWNTs. Inner wall (d) and outer wall (e) diameter distributions as measured from the TEM images shows a mean inner and outer diameter of 1.1 and 1.8 nm, respectively.**

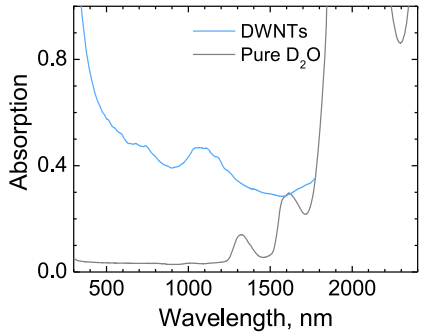


**Figure 2. Absorption spectrum of DWNTs dispersed in $D_2O$ in the 300–1800 nm range. The contribution from $D_2O$ is subtracted. Spectrum of $D_2O$ is also presented.**

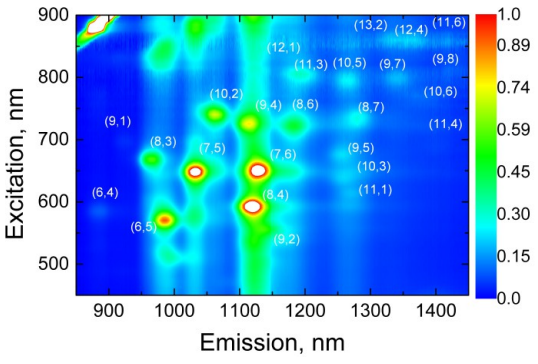


**Figure 3. PLE map for DWNTs dispersed in $D_2O$; (*n*,*m*) is assigned following refs 60 and 69.**

SWNT bundles, which formed aggregations over a 2-month period after they were dispersed in water–SDBS solution. Here, we observe a ~5–7 meV red-shift in $eh_{11}$ and $eh_{22}$ of all the nanotube species compared to the aforementioned aggregated SWNTs. We attribute such red spectral shifts, even larger than those of the aggregated nanotubes,[64,65] to the dielectric screening[75] of the inner tubes by the outer tubes in DWNTs.[62] Such large red-shift could also be due to bundle formation of the individual *s*-SWNTs (*i.e.*, not the inner tubes in DWNTs, but a % of the 8% SWNTs)

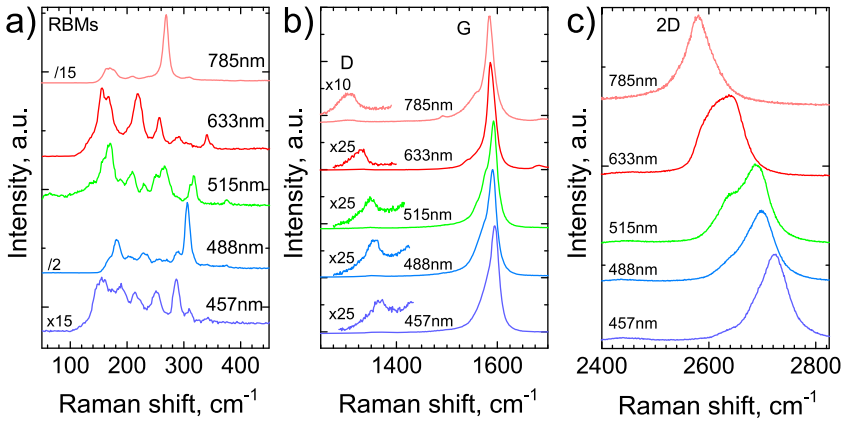


**Figure 4. Raman spectra of DWNTs at different excitation wavelengths: (a) RBM region, (b) G region, and (c) 2D region.**

present in the sample. However, we do not observe significant evidence of bundle formation through strong optical signatures of EET between *s*-nanotubes of similar diameter. In line with our TEM observation, this indicates that the population of individual *s*-SWNTs present in the sample is very low. We argue that the ($eh_{22}$,$eh_{11}$) emission from small tubes comes from the inner *s*-nanotubes of DWNTs which, despite bundling of the DWNTs, have weak EET due to larger physical spacing between themselves (>0.7 nm as opposed to ~0.34 nm in standard SWNT bundles discussed previously[64,65,76]). This is because the EET process between *s*-nanotubes in small bundles occurs *via* Förster resonance energy transfer, whose efficiency is dependent on the inverse sixth power of the physical distance between the donor−acceptor couple.[77] Note that our observation and explanation support PL from inner tubes as observed in previous reports[62,78,79] but contrast reports that the PL emission from the inner tubes in DWNTs is strongly quenched[80] by the outer tubes by up to 4 orders of magnitude.[81] We only detect very weak or no emissions above the 1375 nm range, from tubes with $d_t$ ~1.2−1.3 nm. Indeed, tubes at this $d_t$ range constitute only a very small % of the overall population, as evident from the TEM (Figure 1e,f) and absorption spectra of nanotubes in the dispersion (Figure 2). As discussed later, the nanotube−polymer composite (Figure 6) also shows weak absorption (from $eh_{11}$ excitonic transitions) in the 1400−1600 nm range, that is, for $d_t$ ~1.2−1.3 nm. The outer tubes of the DWNTs with a mean $d_t$ ~1.8 nm are expected to emit in the ~1800−2000 nm range from their $eh_{11}$ excitonic transitions and cannot be measured from their dispersed state in $D_2O$ because of strong optical absorption of $D_2O$ in this range (Figure 2).

Raman spectra of the purified nanotube powder are measured at 457 nm (2.71 eV), 488 nm (2.54 eV), 514.5 nm (2.41 eV), 632.8 nm (1.96 eV), and 785 nm (1.58 eV) to further characterize the nanotubes. In the low frequency region, the radial breathing modes (RBMs) are observed. Their position, Pos(RBM), is inversely related to SWNT diameter, $d_t$,[82−84] as given by Pos(RBM) = $C_1/d_t + C_2$. Combining Pos(RBM) with excitation wavelength and a Kataura plot,[69,85] it is, in principle, possible to derive the SWNT chirality.[86,87] A variety of $C_1$ and $C_2$ values were proposed for this relation.[83,84,87,88] Here, we use $C_1$ = 228.8 $cm^{-1}$ and $C_2$ = 2.4 $cm^{-1}$ from ref 89, derived by plotting the experimental Pos(RBM) to $d_t$ relationship for CVD-grown DWNTs. However, if one is interested in estimation of the band gap, the precise choice of constants is less critical, as the difference in the calculated diameter from the actual value is small. The typical Raman spectrum of nanotubes in the 1500−1600 $cm^{-1}$ region consists of the $G^+$ and $G^-$ bands. In *s*-SWNTs, they originate from the longitudinal (LO) and tangential (TO) modes, respectively, derived from the splitting of the $E_{2g}$ phonon of graphene.[90−92] The positions of the $G^+$ and $G^-$ peaks, Pos($G^+$), Pos($G^-$), are diameter-dependent, and the separation between them increases with decreasing diameter.[91] In *m*-SWNTs, a wide, low frequency $G^-$ is a fingerprint of *m*-SWNTs. On the other hand, the absence of such features does not necessarily imply that only *s*-SWNTs are present but could just signify that *m*-SWNTs are off-resonance.

Thus, a large number of excitation wavelengths are necessary for a complete characterization of nanotubes.[82,88] In particular, we note that ref 93 reported that tubes with up to 100 meV off-resonance from the excitation wavelength can be detected. It is important to note that tubes in resonance with the same laser energy can also have a different diameter.

Figure 4a plots the RBM region for the nanotube samples. Note that the RBM detection range is limited by the cutoff of the notch and edge filters at 140, 160, 150, 130, and 150 $cm^{-1}$ for 457, 488, 514.5, 632.8, and 785 nm, respectively. Thus, we can detect tubes with diameter up to 1.8 nm at 632.8 nm, while we cannot detect tubes with diameter >1.45 nm at 488 nm.

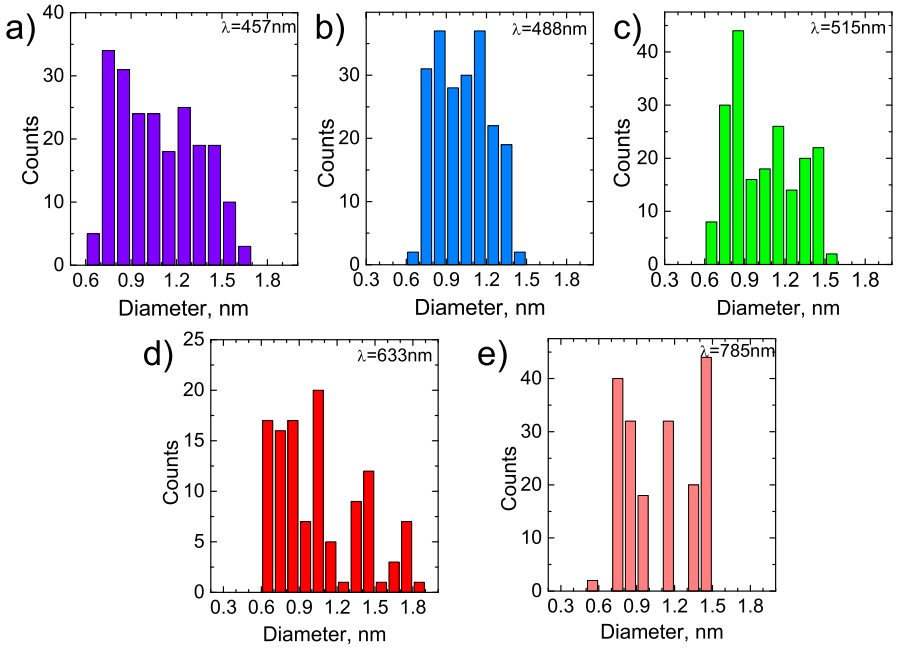


**Figure 5. Diameter analysis from the RBMs of the nanotubes excited by (a) 457, (b) 488, (c) 515, (d) 633, and (e) 785 nm wavelengths, indicating $d_t$ ~0.6−1.8 nm.**

For each excitation wavelength, we use Lorentzians to fit the RBMs from 20 different measurements to derive the statistics presented in Figure 5a−e. The RBM spectra do not reveal a cluster distribution of inner and outer peaks around two well-defined diameters. Rather, they show a broad distribution, spanning the entire range from 140 to 400 $cm^{-1}$. This heterogeneous distribution was also observed in other Raman characterization of CVD-grown DWNTs.[89,94] The counts in Figure 5a−e represent how many times the nanotubes of a particular diameter were observed due to resonance with the excitation wavelength. Keeping this in mind, the RBM results are in agreement with optical absorption and PLE measurements.

Figure 4b,c plots the Raman spectra in the G and 2D region obtained from the nanotube powders, respectively. Very weak D band contributions are also observed in the G region, indicating a small number of defects.[95,96] The $G^+$ and $G^-$ peaks are fitted with Lorentzians. The diameter dependence of $G^+$ and $G^-$ peaks can be used to determine the diameter distribution of the nanotubes.[91] This gives an outer tube diameter range of 1.4−1.8 nm. On the other hand, inner tubes have a diameter distribution in the 0.6−1.0 nm range. The estimation for the inner tubes agrees well with the results of RBMs and the G region. For the case of the outer tubes, we cannot compare with the RBM data due to the cutoff of the notch/edge filter. However, the data agree with the Raman analysis of the G band and TEM, where a distribution of ~1.7 nm is estimated for the outer tubes. The 2D bands in Figure 4c, under different excitations, show a spectral profile with multiple Lorentzian peaks, similar to other reports on DWNTs.[97] Therefore, we expect strong absorption bands at ~1.1 and ~2 $\mu$m from this nanotube sample. This enables us to maximize the change in absorption under strong optical irradiation,[15] making DWNTs ideal SA materials at these wavelengths.

We use the purified nanotubes to prepare nanotube−polymer composites to take the fabrication and integration advantage of polymer photonics into various lightwave systems[15] as well as the optical properties of the constituent ~90% DWNTs. First, the nanotube sample is ultrasonically dispersed in water using SDBS surfactant, centrifuged to remove the large insoluble particles, mixed with aqueous poly(vinyl alcohol) (PVA) solution, and sonicated again to obtain a homogeneous and stable dispersion free of aggregations. We use water as the solvent and SDBS as the surfactant to obtain higher concentration of isolated nanotubes or small bundles[98] than possible with nonaqueous solvents.[99−101] PVA is used for its solvent compatibility. Slow evaporation of water at room temperature produces a freestanding, ~50 $\mu$m thick nanotube−PVA composite (~90% DWNTs, 8% SWNTs, and 2% TWNTs).

Figure 6 shows the optical absorption of the nanotube−polymer composite. This has two absorption bands centered at ~1.1 and ~2 $\mu$m with a peak width of ~250 and ~350 nm, respectively. This corresponds to distinct diameter range $d_t$ ~0.75−1.15 nm ($eh_{11}$ at ~1.1 $\mu$m) and ~1.5−1.9 nm ($eh_{11}$ at ~2 $\mu$m and $eh_{22}$ at ~1.1 $\mu$m),[69] respectively. This matches the inner and outer diameter distributions of the DWNTs. The 8%

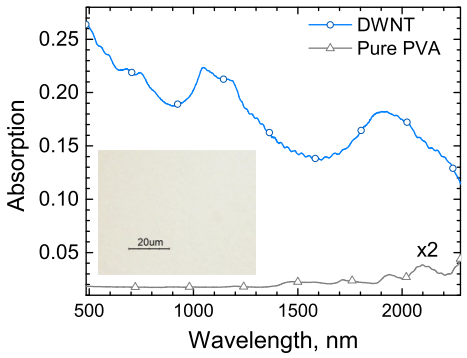


**Figure 6. Absorption spectrum of DWNTs embedded in ~50 $\mu$m PVA polymer composite. The contribution from PVA is subtracted. Absorption spectrum of a pure PVA polymer of the same thickness is also presented. Inset: Optical microscopy of the DWNT–polymer composite reveals no large nanotube aggregation.**

SWNTs present in the sample have a diameter range similar to that of the inner wall of DWNTs. Thus, $eh_{11}$ absorption of these SWNTs also contributes to the strong ~1.1 $\mu$m absorption peak from the $eh_{11}$ of inner and $eh_{22}$ of the outer walls of DWNTs. The inner walls of the 2% TWNTs have diameter ~2 nm as observed by TEM. We do not observe any significant $eh_{11}$ or $eh_{22}$ absorption peaks from the inner walls of the TWNTs. Note that although the $eh_{22}$ excitonic transitions of *s*-SWNTs can extend the operation range of SWNTs to shorter wavelengths,[102] the $eh_{22} \rightarrow eh_{11}$ relaxation is over 1 order of magnitude smaller than $eh_{11} \rightarrow$ ground state relaxation.[103] This increases the $I_{sat}$ at $eh_{22}$ transition by over 1 order of magnitude compared to that at the $eh_{11}$ transition, making the SA device difficult to saturate at the wavelengths corresponding to $eh_{22}$.[102] We argue that the presence of inner walls in DWNTs and strong contribution from their $eh_{11}$ transition at 1.1 $\mu$m contribution ensures $I_{sat}$ comparable to that of the SWNTs. Similarly, MWNTs, as discussed before, also have high saturation intensity,[49,50] which limits their SA applicability.

Small aggregation of CNTs (<1 $\mu$m), in general, is considered beneficial for saturable absorption. Indeed, such level of bundling improves carrier relaxation times by up to an order of magnitude[104] by providing multiple relaxation pathways for the excited carriers.[105] However, these bundles/aggregates are beyond the standard optical microscope resolution limit. Thus, typical optical microscopy is usually used to identify samples with large (>1 $\mu$m) aggregates, which are more likely to exhibit large scattering (*i.e.*, nonsaturable) losses.[15] Optical microscopy (Figure 6, inset) reveals no large nanotube aggregations or defects in the composite, thus avoiding such losses.[106]

The polymeric film-based device is integrated by taking a ~2 mm$^2$ nanotube–polymer composite, sandwiching it between a fiber pigtailed fiber connector with physical contact (FC/PC) with index matching gel at both the fiber ends. The index matching gel is used to reduce the insertion losses. The SA device is used to demonstrate mode-locking at 1, 1.5, and ~2.0 $\mu$m. The fundamental working principle for the nanotube-based SA devices is explained in refs 15 and 42.

Figure 7a shows the setup for 1 $\mu$m. A 2 m Yb-doped fiber-based optical amplifier is used to provide gain for lasing. This is a commercial IPG amplifier unit with 25 dB gain at the signal wavelength. A polarization controller is employed for mode-locking optimization. A fused 20/80 coupler is utilized as the output coupler. The 20% port is used for the measurements. All of the cavity fiber has positive group velocity dispersion (GVD) ($\beta_2 \approx 18$ ps$^2$ km$^{-1}$). A circulator and chirped fiber Bragg grating are inserted inside the ring cavity to set the overall GVD negative, to facilitate soliton-like pulse shaping through the interplay of group velocity dispersion and self-phase modulation.[109] The total cavity length is ~12.5 m.

Stable mode-locking at 1 $\mu$m is achieved. No pulses are observed after removing the composite from the cavity, confirming that mode-locking is initiated by the DWNT composite. Figure 7b plots a typical second harmonic generation autocorrelation trace, which is well fitted by a sech$^2$ temporal profile. This gives a full width at half-maximum (FWHM) pulse duration of 4.85 ps. Such broad pulse is mainly caused by large overall negative GVD.[109] The output spectral data are shown in Figure 7c. The output spectrum peaks at 1066 nm with FWHM = 0.284 nm. The sidebands are typical of soliton operation; due to intracavity periodical perturbations,[108] the asymmetry can be attributed to the significant third-order dispersion introduced by the chirped fiber Bragg grating.[108,109] The time–bandwidth product (TBP) of the output pulses is 0.36. The deviation from TBP = 0.31 expected for transform-limited sech$^2$ pulses[109] indicates the presence of minor chirping of the output pulses.[109] The output repetition rate is ~16.37 MHz. Typical output power is 0.12 mW, with single pulse energy of 7.3 pJ. These results are comparable to those obtained with SWNTs at 1 $\mu$m.[23,24]

For 1.5 $\mu$m operation, we use an erbium-doped fiber (EDF) as the gain medium, pumped by a 980 nm diode laser *via* a wavelength division multiplexer (WDM). An isolator is employed after the gain fiber to ensure unidirectional operation. A polarization controller is used for mode-locking optimization. The 20% tap of the 20/80 coupler is used as output for measurement. The setup is presented in Figure 8a. The length of EDF is 0.8 m. The gain fiber has a ~6/125 $\mu$m core/cladding geometry and has an absorption of ~40 dB/m at a wavelength of 1531 nm. The total cavity length is 7.3 m. The output pulse duration is around 532 fs, assuming sech$^2$ pulse profile; see Figure 8b. The TBP of the output pulses at 1.5 $\mu$m is 0.42. The deviation from TBP = 0.31 is due to the minor chirping of the output pulses. In this case, the peak lasing wavelength is 1559 nm, with

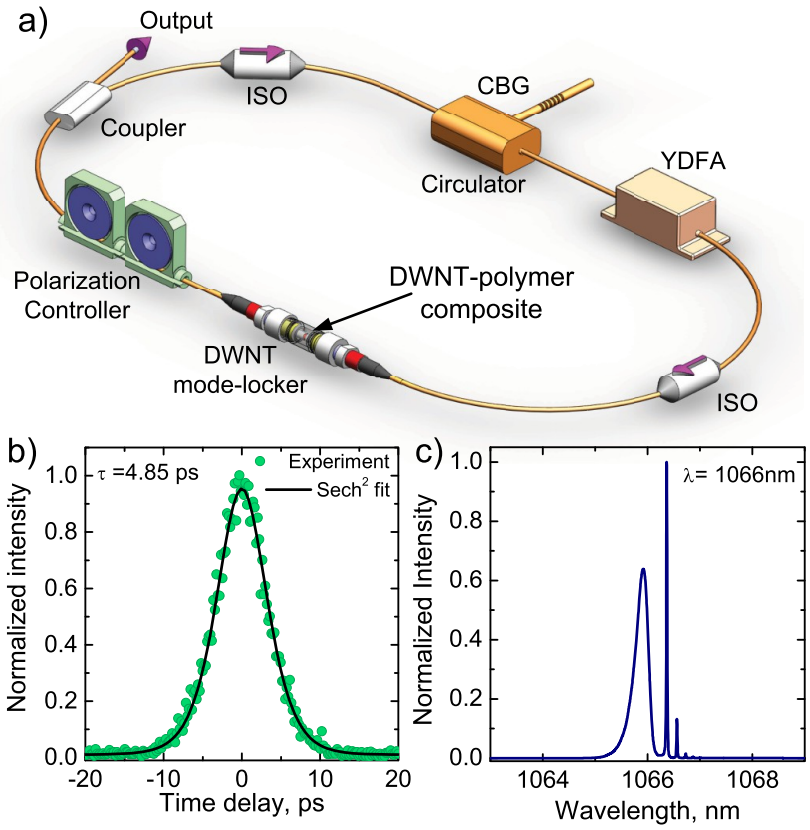


**Figure 7. (a) Laser setup at 1 $\mu$m. ISO, isolator; CBG, chirped Bragg grating; YDFA, Yb-doped fiber amplifier; PC, polarization controller. The DWNT polymer composite is sandwiched between the fiber connectors. (b) Second harmonic generation autocorrelation trace of the output pulses at 1 $\mu$m. (c) Output spectrum.**

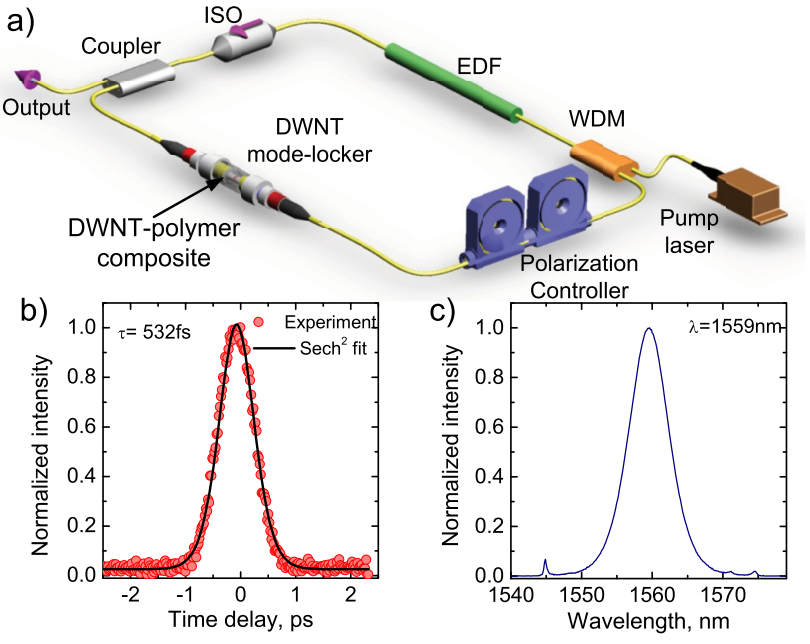


**Figure 8. (a) Laser setup at 1.5 $\mu$m. EDF, erbium-doped fiber; WDM, wavelength division multiplexer. (b) Second harmonic generation autocorrelation trace of mode-locked pulses at 1.5 $\mu$m. (c) Output spectrum.**

FWHM = 6.5 nm. Typical soliton sidebands are also observed. The sideband intensity difference is mainly because of higher EDF gain at ~1545 nm compared to that at ~1570 nm.[107,108]

For ~2.0 $\mu$m operation, we construct a ring laser cavity using a 3.5 m long Tm-doped silica fiber as the gain medium. The gain fiber is a single clad thulium-doped fiber from Nufern. It has a 9 $\mu$m/125 $\mu$m

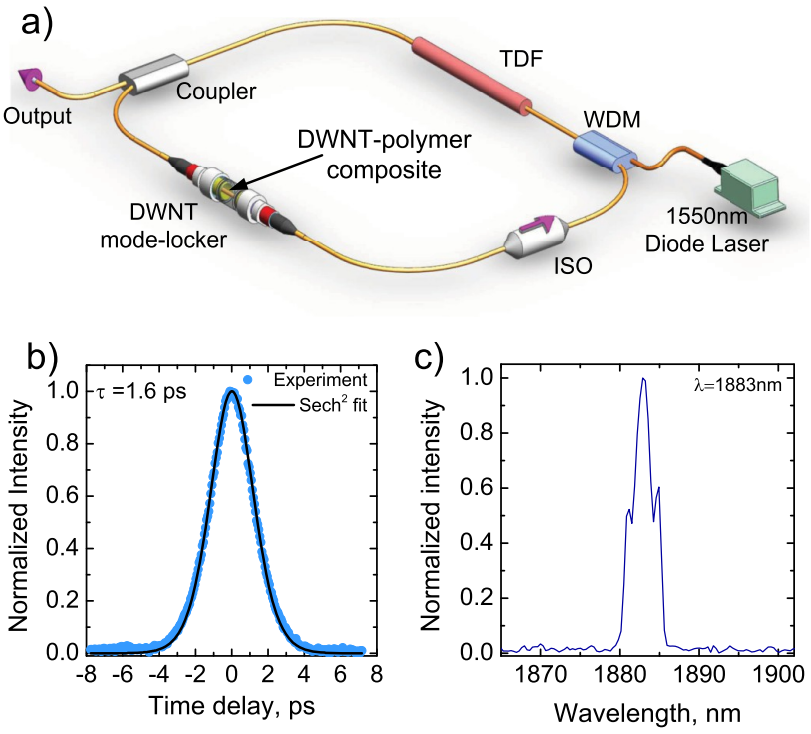


**Figure 9. (a) Laser setup at ~2 $\mu$m. TDF, thulium-doped fiber. (b) Second harmonic generation autocorrelation trace of mode-locked pulses at ~2 $\mu$m. (c) Output spectrum.**

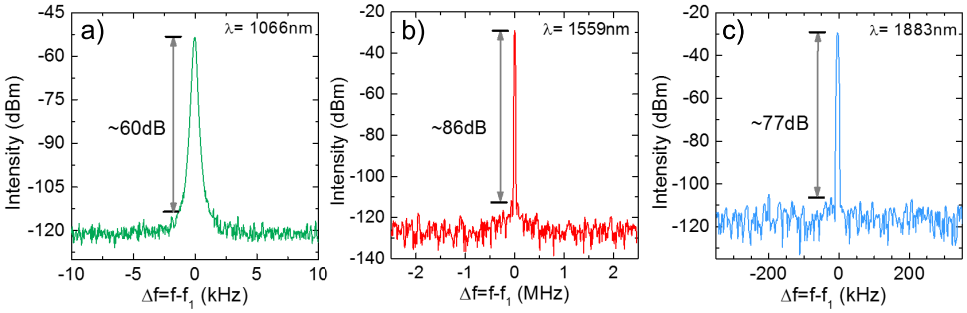


**Figure 10. RF spectrum measured around the fundamental repetition rate: (a) $f_1$ = 16.37 MHz, (b) $f_1$ = 27.4 MHz, (c) $f_1$ = 17.82 MHz showing peak to pedestal extinction ratios >60 dB in all three wavelengths.**

core/cladding geometry and has an absorption of ~10 dB/m at 1560 nm. An amplified 1560 nm diode laser through a WDM pumps the gain fiber. A coupler is used to couple 50% light back into the cavity while guiding 50% of the incident power to the output port of the laser. The mode-locker device is on one end, connected to the wide-band coupler and on the other end, spliced to an isolator to ensure unidirectional light propagation (Figure 9a). A dichroic mirror is used to eliminate the residual pump power at 1560 nm. At ~350 mW pump power, we achieve an output power of ~1.2 mW. The autocorrelation trace is shown in Figure 9b, which closely follows a sech$^2$ shape. The mode-locked optical spectrum in Figure 9c exhibits a center wavelength of 1883 nm with a FWHM spectral width of ~3.2 nm. Typical sidebands are due to periodic perturbations from cavity components. The corresponding TBP is ~0.44, which again indicates the presence of chirping. The repetition rate for the output pulse train is 17.82 MHz, as determined by the cavity length of ~10.8 m.

Radio frequency (rf) spectrum measurements can be used to monitor the mode-locking stability.[110] The typical rf spectra at 1, 1.5, and 2 $\mu$m have a peak at an output repetition rate corresponding to the cavity round trip time (Figure 10). This confirms reliable continuous-wave mode-locking.[111] For the rf spectrum at 1066, 1559, and 1883 nm, the peak to pedestal extinction ratios are ~60, 86, and 77 dB, respectively (>10$^6$ contrast). This confirms a stable output pulse.[111]

## CONCLUSIONS

Our demonstration of wide-band mode-locking optical pulses at 1, 1.5, and 2 $\mu$m using DWNT–polymer

composites shows that they could potentially be useful for wide-band ultrafast photonic applications. In particular, building on our experiments, few-wall (*e.g.*, <5) nanotubes (FWNTs) with broader absorption profile and $I_{sat}$ lower than large diameter FWNTs may become very attractive for wide-band mid-infrared applications.

## EXPERIMENTAL METHODS

**Transmission Electron Microscopy.** For TEM analysis, dispersions are drop-cast onto a lacey carbon support grid (400 mesh). Water is readily removed by an absorbent underneath, leaving DWNTs on the carbon grid. TEM images are taken using a JEM-3000F FEGTEM at 300 kV.

**Raman and Optical Absorption Spectroscopy.** Raman spectroscopy measurements are carried out using a Renishaw inVia spectrometer using a 50× objective. A PerkinElmer Lambda 950 spectrophotometer is used for the vis–NIR absorption measurements with 1 nm step.

**Preparation of DWNT Dispersions for Photoluminescence Excitation Spectroscopy.** Purified DWNTs (0.01 wt %) are ultrasonicated with 0.2 wt % of SDBS in 10 mL of $D_2O$ inside a sealed glass test tube in a bath sonicator (Bioruptor; Diagenode) at 270 W, 20 kHz for 4 h. The homogeneous dispersion is then centrifuged in a TH-641 rotor using a sorvall WX 100 ultracentrifuge at ~200 000*g* for 2 h and the top 30% decanted for PLE characterization.

**Photoluminescence Excitation Spectroscopy.** The PLE maps are taken from nanotube dispersions in a HORIBA Jobin Yvon excitation–emission spectrofluorometer (Fluorolog-3) equipped with a xenon lamp excitation source and a liquid-nitrogen-cooled InGaAs detector (Symphony solo). The PLE maps are measured at right angle scattering by scanning the excitation wavelength from 300 to 900 nm with 5 nm steps and 60 s exposure for ~850 to ~1450 nm emission range. The entrance and exit slit widths are 14 and 30 nm, respectively.

**Preparation of DWNT–PVA Composites.** Purified DWNTs (0.04 wt %) grown by CCVD method[71] are ultrasonicated in 10 mL of DI water with 1 wt % of SDBS using a tip sonicator (Branson 450A, 20 kHz) at ~100 W output power and 10 °C temperature for 4 h. The homogeneous dispersion is centrifuged at ~100 000*g* for 30 min in a TH-641 rotor using a sorvall WX100 ultracentrifuge. The top 60% of the dispersion is then decanted. Then, 4 mL of this dispersion is mixed with a 1 wt % aqueous solution of 120 mg of PVA and is ultrasonicated again for 30 min. The homogeneous mixture has a viscosity of 1.6 mPa·s at 25 °C, measured using a TA Instruments Discovery HR-1 rheometer. This low viscosity mixture is then drop-cast and the solvent slowly evaporated at room temperature in a desiccator, resulting in a ~50 $\mu$m freestanding DWNT–PVA composite.

**Characterization of Mode-Locked Pulses.** The pump and average output power are monitored by a power meter. The pulse duration and spectrum are recorded using a second harmonic generation (SHG) intensity autocorrelator and an optical spectrum analyzer, respectively. To study the operation stability, we measure the rf spectrum using a photodetector connected to a spectrum analyzer.

*Conflict of Interest:* The authors declare no competing financial interest.

*Acknowledgment.* We thank R.C.T. Howe for the viscosity measurements. We acknowledge funding from EPSRC GR/S97613/01, EP/E500935/1, the ERC Grant NANOPOTS, a Royal Society Brian Mercer Award for Innovation. A.C.F. is a Royal Society Wolfson Research Merit Award holder. V.N. wishes to acknowledge support from the European Research Council (ERC Starting Grant 2DNanoCaps) and Science Foundation Ireland, P.T. from National Natural Science Foundation of China, Grants No. 11225421, F.B. from the Newton International Fellowship, Z.S. from Teknologiateollisuus TT-100, the European Union's Seventh Framework Programme (No. 631610), and Aalto University, T.H. from NSFC (Grant No. 61150110487), and the Royal Academy of Engineering (Graphlex).

## REFERENCES AND NOTES

1. O'Mahony, M. J.; Politi, C.; Klonidis, D.; Nejabati, R.; Simeonidou, D. Future Optical Networks. *J. Lightwave Technol.* **2006**, *24*, 4684–4696.
2. Leclerc, O.; Lavigne, B.; Balmefrezol, E.; Brindel, P.; Pierre, L.; Rouvillain, D.; Seguineau, F. Optical Regeneration at 40 Gb/s and Beyond. *J. Lightwave Technol.* **2003**, *21*, 2779–2790.
3. Simon, J.; Bramerie, L.; Ginovart, F.; Roncin, V.; Gay, M.; Feve, S.; le Cren, E.; Chares, M. All-Optical Regeneration Techniques. *Ann. Telecommun.* **2003**, *58*, 1708–1724.
4. Rouvillain, D.; Brindel, P.; Seguineau, F.; Pierre, L.; Leclerc, O.; Choumane, H.; Aubin, G.; Oudar, J. L. Optical 2R Regenerator Based on Passive Saturable Absorber for 40Gbit/s WDM Long-Haul Rransmissions. *Electron. Lett.* **2002**, *38*, 1113–1114.
5. Hirano, A.; Kobayashi, H.; Tsuda, H.; Takahashi, R.; Asobe, M.; Sato, K.; Hagimoto, K. 10 Gbit/s RZ All-Optical Discrimination Using Refined Saturable Absorber Optical Gate. *Electron. Lett.* **1998**, *34*, 198–199.
6. Jin, C. Y.; Kojima, O.; Inoue, T.; Kita, T.; Wada, O.; Hopkinson, M.; Akahane, K. Detailed Design and Characterization of All-Optical Switches Based on InAs/GaAs Quantum Dots in a Vertical Cavity. *IEEE J. Quantum Electron.* **2010**, *46*, 1582–1589.
7. Guina, M. D.; Vainionpaa, A. M.; Orsila, L.; Harkonen, A.; Lyytikainen, J.; Gomes, L. A.; Okhotnikov, O. G. Saturable Absorber Intensity Modulator. *IEEE J. Quantum Electron.* **2003**, *39*, 1143–1149.
8. Arecchi, F.; Degiorgio, V.; Sona, A. A Crossed-Beam Optical Gate with a Saturable Absorber. *Nuovo Cimento* **1965**, *38*, 1096–1098.
9. Land, T. A.; Michely, T.; Behm, R. J.; Hemminger, J. C.; Comsa, G. STM Investigation of Single Layer Graphite Structures Produced on Pt(111) by Hydrocarbon Decomposition. *Surf. Sci.* **1992**, *264*, 261–270.
10. Reid, D.; Maguire, P. J.; Barry, L. P.; Le, Q.-T.; Lobo, S.; Gay, M.; Bramerie, L.; Joindot, M.; Simon, J.-C.; Massoubre, D.; *et al.* All-Optical Sampling and Spectrographic Pulse Measurement Using Cross-Absorption Modulation in Multiple-Quantum-Well Devices. *J. Opt. Soc. Am. B* **2008**, *25*, A133–A139.
11. Clarke, A. M.; Anandarajah, P. M.; Bramerie, L.; Guignard, C.; Maher, R.; Massoubre, D.; Shen, A.; Oudar, J. L.; Barry, L. P.; Simon, J. C. 80-Gb/s OTDM System Analysis of a Vertical Microcavity-Based Saturable Absorber for the Enhancement of Pulse Pedestal Suppression. *IEEE Photonics Technol. Lett.* **2007**, *19*, 321–323.
12. Keller, U. Recent Developments in Compact Ultrafast Lasers. *Nature* **2003**, *424*, 831–838.
13. Okhotnikov, O.; Grudinin, A.; Pessa, M. Ultra-fast Fibre Laser Systems Based on SESAM Technology: New Horizons and Applications. *New J. Phys.* **2004**, *6*, 177.
14. Keller, U.; Tropper, A. C. Passively Modelocked Surface-Emitting Semiconductor Lasers. *Phys. Rep.* **2006**, *429*, 67–120.
15. Hasan, T.; Sun, Z.; Wang, F.; Bonaccorso, F.; Tan, P. H.; Rozhin, A. G.; Ferrari, A. C. Nanotube–Polymer Composites for Ultrafast Photonics. *Adv. Mater.* **2009**, *21*, 3874–3899.
16. Set, S. Y.; Yaguchi, H.; Tanaka, Y.; Jablonski, M. Ultrafast Fiber Pulsed Lasers Incorporating Carbon Nanotubes. *IEEE J. Sel. Top. Quantum Electron.* **2004**, *10*, 137–146.
17. Sun, Z.; Rozhin, A. G.; Wang, F.; Hasan, T.; Popa, D.; O'Neill, W.; Ferrari, A. C. A Compact, High Power, Ultrafast Laser Mode-Locked by Carbon Nanotubes. *Appl. Phys. Lett.* **2009**, *95*, 253102.

18. Sun, Z.; Rozhin, A. G.; Wang, F.; Scardaci, V.; Milne, W. I.; White, I. H.; Hennrich, F.; Ferrari, A. C. L-Band Ultrafast Fiber Laser Mode Locked by Carbon Nanotubes. *Appl. Phys. Lett.* **2008**, *93*, 061114.
19. Chen, Y.-C.; Raravikar, N. R.; Schadler, L. S.; Ajayan, P. M.; Zhao, Y.-P.; Lu, T.-M.; Wang, G.-C.; Zhang, X.-C. Ultrafast Optical Switching Properties of Single-Wall Carbon Nanotube Polymer Composites at 1.55 $\mu$m. *Appl. Phys. Lett.* **2002**, *81*, 975–977.
20. Scardaci, V.; Sun, Z.; Wang, F.; Rozhin, A. G.; Hasan, T.; Hennrich, F.; White, I. H.; Milne, W. I.; Ferrari, A. C. Carbon Nanotube-Polycarbonate Composites for Ultrafast Lasers. *Adv. Mater.* **2008**, *20*, 4040–4043.
21. Wang, F.; Rozhin, A. G.; Scardaci, V.; Sun, Z.; Hennrich, F.; White, I. H.; Milne, W. I.; Ferrari, A. C. Wideband-Tuneable, Nanotube Mode-Locked, Fibre Laser. *Nat. Nanotechnol.* **2008**, *3*, 738–742.
22. Beecher, S. J.; Thomson, R. R.; Psaila, N. D.; Sun, Z.; Hasan, T.; Rozhin, A. G.; Ferrari, A. C.; Kar, A. K. 320 fs Pulse Generation from an Ultrafast Laser Inscribed Waveguide Laser Mode-Locked by a Nanotube Saturable Absorber. *Appl. Phys. Lett.* **2010**, *97*, 111114.
23. Kelleher, E. J. R.; Travers, J. C.; Ippen, E. P.; Sun, Z.; Ferrari, A. C.; Popov, S. V.; Taylor, J. R. Generation and Direct Measurement of Giant Chirp in a Passively Mode-Locked Laser. *Opt. Lett.* **2009**, *34*, 3526–3528.
24. Kelleher, E. J. R.; Travers, J. C.; Sun, Z.; Rozhin, A. G.; Ferrari, A. C.; Popov, S. V.; Taylor, J. R. Nanosecond-Pulse Fiber Lasers Mode-Locked with Nanotubes. *Appl. Phys. Lett.* **2009**, *95*, 111108.
25. Martinez, A.; Zhou, K.; Bennion, I.; Yamashita, S. Passive Mode-Locked Lasing by Injecting a Carbon Nanotube-Solution in the Core of an Optical Fiber. *Opt. Express* **2010**, *18*, 11008–11014.
26. Popa, D.; Sun, Z.; Hasan, T.; Cho, W. B.; Wang, F.; Torrisi, F.; Ferrari, A. C. 74-fs Nanotube-Mode-Locked Fiber Laser. *Appl. Phys. Lett.* **2012**, *101*, 153107.
27. Mary, R.; Brown, G.; Beecher, S.; Thomson, R.; Popa, D.; Sun, Z.; Torrisi, F.; Hasan, T.; Milana, S.; Bonaccorso, F.; *et al.* Evanescent-Wave Coupled Right Angled Buried Waveguide: Applications in Carbon Nanotube Mode-Locking. *Appl. Phys. Lett.* **2013**, *103*, 221117.
28. Martinez, A.; Sun, Z. Nanotube and Graphene Saturable Absorbers for Fibre Lasers. *Nat. Photonics* **2013**, *7*, 842–845.
29. Sun, Z.; Hasan, T.; Torrisi, F.; Popa, D.; Privitera, G.; Wang, F.; Bonaccorso, F.; Basko, D. M.; Ferrari, A. C. Graphene Mode-Locked Ultrafast Laser. *ACS Nano* **2010**, *4*, 803–810.
30. Popa, D.; Sun, Z.; Torrisi, F.; Hasan, T.; Wang, F.; Ferrari, A. C. Sub 200 fs Pulse Generation from a Graphene Mode-Locked Fiber Laser. *Appl. Phys. Lett.* **2010**, *97*, 203106.
31. Sun, Z.; Popa, D.; Hasan, T.; Torrisi, F.; Wang, F.; Kelleher, E. J. R.; Travers, J. C.; Nicolosi, V.; Ferrari, A. C. A Stable, Wideband Tunable, Near Transform-Limited, Graphene-Mode-Locked, Ultrafast Laser. *Nano Res.* **2010**, *3*, 653–660.
32. Hasan, T.; Torrisi, F.; Sun, Z.; Popa, D.; Nicolosi, V.; Privitera, G.; Bonaccorso, F.; Ferrari, A. C. Solution-Phase Exfoliation of Graphite for Ultrafast Photonics. *Phys. Status Solidi B* **2010**, *247*, 2953–2957.
33. Martinez, A.; Fuse, K.; Xu, B.; Yamashita, S. Optical Deposition of Graphene and Carbon Nanotubes in a Fiber Ferrule for Passive Mode-Locked Lasing. *Opt. Express* **2010**, *18*, 23054–23061.
34. Tan, W. D.; Su, C. Y.; Knize, R. J.; Xie, G. Q.; Li, L. J.; Tang, D. Y. Mode Locking of Ceramic Nd:Yttrium Aluminum Garnet with Graphene as a Saturable Absorber. *Appl. Phys. Lett.* **2010**, *96*, 031106.
35. Zhang, H.; Tang, D.; Knize, R. J.; Zhao, L.; Bao, Q.; Loh, K. P. Graphene Mode Locked, Wavelength-Tunable, Dissipative Soliton Fiber Laser. *Appl. Phys. Lett.* **2010**, *96*, 111112.
36. Sun, Z.; Hasan, T.; Ferrari, A. C. Ultrafast Lasers Mode-Locked by Nanotubes and Graphene. *Physica E* **2012**, *44*, 1082–1091.
37. Popa, D.; Sun, Z.; Hasan, T.; Torrisi, F.; Wang, F.; Ferrari, A. C. Graphene Q-Switched, Tunable Fiber Laser. *Appl. Phys. Lett.* **2011**, *98*, 073106.
38. Mary, R.; Brown, G.; Beecher, S. J.; Torrisi, F.; Milana, S.; Popa, D.; Hasan, T.; Sun, Z.; Lidorikis, E.; Ohara, S.; *et al.* 1.5 GHz Picosecond Pulse Generation from a Monolithic Waveguide Laser with a Graphene-Film Saturable Output Coupler. *Opt. Express* **2013**, *21*, 7943–7950.
39. Fu, B.; Hua, Y.; Xiao, X.; Zhu, H.; Sun, Z.; Yang, C. Broadband Graphene Saturable Absorber for Pulsed Fiber Lasers at 1, 1.5 and 2 $\mu$m. *IEEE J. Sel. Top. Quantum Electron.* **2014**, 10.1109/JSTQE.2014.2302361.
40. Zaugg, C. A.; Sun, Z.; Wittwer, V. J.; Popa, D.; Milana, S.; Kulmala, T. S.; Sundaram, R. S.; Mangold, M.; Sieber, O. D.; Golling, M.; *et al.* Ultrafast and Widely Tuneable Vertical-External-Cavity Surface-Emitting Laser, Mode-Locked by a Graphene-Integrated Distributed Bragg Reflector. *Opt. Express* **2013**, *21*, 31548–31559.
41. Kivistö, S.; Hakulinen, T.; Kaskela, A.; Aitchison, B.; Brown, D. P.; Nasibulin, A. G.; Kauppinen, E. I.; Härkönen, A.; Okhotnikov, O. G. Carbon Nanotube Films for Ultrafast Broadband Technology. *Opt. Express* **2009**, *17*, 2358–2363.
42. Hasan, T.; Scardaci, V.; Tan, P. H.; Bonaccorso, F.; Rozhin, A. G.; Sun, Z.; Ferrari, A. C. In *Molecular- and Nano-Tubes*; Hayden, O., Nielsch, K., Eds.; Springer: New York, 2011.
43. Bonaccorso, F.; Sun, Z.; Hasan, T.; Ferrari, A. C. Graphene Photonics and Optoelectronics. *Nat. Photonics* **2010**, *4*, 611–622.
44. Boyd, R. W. *Nonlinear Optics*; Academic Press: San Diego, CA, 2003.
45. Zitter, R. N. Saturated Optical Absorption through Band Filling in Semiconductors. *Appl. Phys. Lett.* **1969**, *14*, 73–74.
46. Cho, W. B.; Kim, J. W.; Lee, H. W.; Bae, S.; Hong, B. H.; Choi, S. Y.; Baek, I. H.; Kim, K.; Yeom, D.-I.; Rotermund, F. High-Quality, Large-Area Monolayer Graphene for Efficient Bulk Laser Mode-Locking near 1.25$\mu$m. *Opt. Lett.* **2011**, *36*, 4089–4091.
47. Xing, G.; Guo, H.; Zhang, X.; Sum, T. C.; Huan, C. H. A. The Physics of Ultrafast Saturable Absorption in Graphene. *Opt. Express* **2010**, *18*, 4564–4573.
48. Kamaraju, N.; Kumar, S.; Kim, Y. A.; Hayashi, T.; Muramatsu, H.; Endo, M.; Sood, A. K. Double Walled Carbon Nanotubes as Ultrafast Optical Switches. *Appl. Phys. Lett.* **2009**, *95*, 081106.
49. Elim, H. I.; Ji, W.; Ma, G. H.; Lim, K. Y.; Sow, C. H.; Huan, C. H. A. Ultrafast Absorptive and Refractive Nonlinearities in Multiwalled Carbon Nanotube Films. *Appl. Phys. Lett.* **2004**, *85*, 1799–1801.
50. Lim, S. H.; Elim, H. I.; Gao, X. Y.; Wee, A. T. S.; Ji, W.; Lee, J. Y.; Lin, J. Electronic and Optical Properties of Nitrogen-Doped Multiwalled Carbon Nanotubes. *Phys. Rev. B* **2006**, *73*, 045402.
51. Zhang, L.; Wang, Y.; Yu, H.; Sun, L.; Hou, W.; Lin, X.; Li, J. Passive Mode-Locked Nd:$YVO_4$ Laser Using a Multi-walled Carbon Nanotube Saturable Absorber. *Laser Phys.* **2011**, *21*, 1382–1386.
52. Shen, C.; Brozena, A. H.; Wang, Y. H. Double-Walled Carbon Nanotubes: Challenges and Opportunities. *Nanoscale* **2011**, *3*, 503–518.
53. Piao, Y.; Chen, C.-F.; Green, A. A.; Kwon, H.; Hersam, M. C.; Lee, C. S.; Schatz, G. C.; Wang, Y. Optical and Electrical Properties of Inner Tubes in Outer Wall-Selectively Functionalized Double-Wall Carbon Nanotubes. *J. Phys. Chem. Lett.* **2011**, *2*, 1577–1582.
54. Jariwala, D.; Sangwan, V. K.; Lauhon, L. J.; Marks, T. J.; Hersam, M. C. Carbon Nanomaterials for Electronics, Optoelectronics, Photovoltaics, And Sensing. *Chem. Soc. Rev.* **2013**, *42*, 2824–2860.
55. Kamaraju, N.; Kumar, S.; Karthikeyan, B.; Moravsky, A.; Loutfy, R. O.; Sood, A. K. Ultrafast Electron Dynamics and Cubic Optical Nonlinearity of Freestanding Thin Film of Double Walled Carbon Nanotubes. *Appl. Phys. Lett.* **2008**, *93*, 091903.
56. Nakamura, A.; Tomikawa, T.; Watanabe, M.; Hamanaka, Y.; Saito; Ago, H. Non-linear Optical Response and Relaxation Dynamics in Double-Walled Carbon Nanotubes. *J. Lumin.* **2006**, *119–120*, 8–12.
57. Nakamura, A.; Hikosaka, N.; Imamura, S.; Takahashi, Y.; Ago, H.; Kishida, H. Third-Order Nonlinear Optical

Response in Double-Walled Carbon Nanotubes. *J. Lumin.* **2009**, *129*, 1722–1725.
58. Kalbac, M.; Green, A. A.; Hersam, M. C.; Kavan, L. Probing Charge Transfer between Shells of Double-Walled Carbon Nanotubes Sorted by Outer-Wall Electronic Type. *Chem.—Eur. J.* **2011**, *17*, 9806–9815.
59. Chen, G.; Bandow, S.; Margine, E. R.; Nisoli, C.; Kolmogorov, A. N.; Crespi, V. H.; Gupta, R.; Sumanasekera, G. U.; Iijima, S.; Eklund, P. C. Chemically Doped Double-Walled Carbon Nanotubes: Cylindrical Molecular Capacitors. *Phys. Rev. Lett.* **2003**, *90*, 257403.
60. Hertel, T.; Hagen, A.; Talalaev, V.; Arnold, K.; Hennrich, F.; Kappes, M.; Rosenthal, S.; McBride, J.; Ulbricht, H.; Flahaut, E. Spectroscopy of Single- and Double-Wall Carbon Nanotubes in Different Environments. *Nano Lett.* **2005**, *5*, 511–514.
61. Blau, W. J.; Wang, J. Optical Materials: Variety Pays Off for Nanotubes. *Nat. Nanotechnol.* **2008**, *3*, 705–706.
62. Hirori, H.; Matsuda, K.; Kanemitsu, Y. Exciton Energy Transfer between the Inner and Outer Tubes in Double-Walled Carbon Nanotubes. *Phys. Rev. B* **2008**, *78*, 113409.
63. Koyama, T.; Miyata, Y.; Asaka, K.; Shinohara, H.; Saito, Y.; Nakamura, A. Ultrafast Energy Transfer of One-Dimensional Excitons between Carbon Nanotubes: A Femtosecond Time-Resolved Luminescence Study. *Phys. Chem. Chem. Phys.* **2012**, *14*, 1070–1084.
64. Tan, P. H.; Rozhin, A. G.; Hasan, T.; Hu, P.; Scardaci, V.; Milne, W. I.; Ferrari, A. C. Photoluminescence Spectroscopy of Carbon Nanotube Bundles: Evidence for Exciton Energy Transfer. *Phys. Rev. Lett.* **2007**, *99*, 137402.
65. Tan, P. H.; Hasan, T.; Bonaccorso, F.; Scardaci, V.; Rozhin, A. G.; Milne, W. I.; Ferrari, A. C. Optical Properties of Nanotube Bundles by Photoluminescence Excitation and Absorption Spectroscopy. *Physica E* **2008**, *40*, 2352–2359.
66. Iakoubovskii, K.; Minami, N.; Ueno, T.; Kazaoui, S.; Kataura, H. Optical Characterization of Double-Wall Carbon Nanotubes: Evidence for Inner Tube Shielding. *J. Phys. Chem. C* **2008**, *112*, 11194–11198.
67. Pfeiffer, R.; Pichler, T.; Kim, Y.; Kuzmany, H. *Topics in Applied Physics*; Springer: Berlin, 2008; Vol. 111.
68. Pfeiffer, R.; Kuzmany, H.; Kramberger, C.; Schaman, C.; Pichler, T.; Kataura, H.; Achiba, Y.; Kürti, J.; Zólyomi, V. Unusual High Degree of Unperturbed Environment in the Interior of Single-Wall Carbon Nanotubes. *Phys. Rev. Lett.* **2003**, *90*, 225501.
69. Liu, K.; Deslippe, J.; Xiao, F.; Capaz, R. B.; Hong, X.; Aloni, S.; Zettl, A.; Wang, W.; Bai, X.; Louie, S. G. An Atlas of Carbon Nanotube Optical Transitions. *Nat. Nanotechnol.* **2012**, *7*, 325–329.
70. Ilev, I.; Waynant, R. In *Mid-Infrared Semiconductor Optoelectronics*; Krier, A., Ed.; Springer: Berlin, 2006.
71. Sandler, J.; Kirk, J.; Kinloch, I.; Shaffer, M.; Windle, A. Ultra-low Electrical Percolation Threshold in Carbon-Nanotube-Epoxy Composites. *Polymer* **2003**, *44*, 5893–5899.
72. Grady, B. P. *Carbon Nanotube—Polymer Composites: Manufacture, Properties, and Applications*; Wiley: New York, 2011.
73. Flahaut, E.; Bacsa, R.; Peigney, A.; Laurent, C. Gram-Scale CCVD Synthesis of Double-Walled Carbon Nanotubes. *Chem. Commun.* **2003**, 1442–1443.
74. Osswald, S.; Flahaut, E.; Gogotsi, Y. *In Situ* Raman Spectroscopy Study of Oxidation of Double- and Single-Wall Carbon Nanotubes. *Chem. Mater.* **2006**, *18*, 1525–1533.
75. Walsh, A. G.; Vamivakas, A. N.; Yin, Y.; Unlü, M. S.; Goldberg, B. B.; Swan, A. K.; Cronin, S. B. Screening of Excitons in Single, Suspended Carbon Nanotubes. *Nano Lett.* **2007**, *7*, 1485–1488.
76. Qian, H.; Georgi, C.; Anderson, N.; Green, A. A.; Hersam, M. C.; Novotny, L.; Hartschuh, A. Exciton Energy Transfer in Pairs of Single-Walled Carbon Nanotubes. *Nano Lett.* **2008**, *8*, 1363–1367.
77. Förster, T. Transfer Mechanisms of Electronic Excitation. *Discuss. Faraday Soc.* **1959**, *27*, 7–17.
78. Hayashi, T.; Shimamoto, D.; Kim, Y. A.; Muramatsu, H.; Okino, F.; Touhara, H.; Shimada, T.; Miyauchi, Y.; Maruyama, S.; Terrones, M.; *et al.* Selective Optical Property Modification of Double-Walled Carbon Nanotubes by Fluorination. *ACS Nano* **2008**, *2*, 485–488.
79. Kim, J. H.; Kataoka, M.; Shimamoto, D.; Muramatsu, H.; Jung, Y. C.; Hayashi, T.; Kim, Y. A.; Endo, M.; Park, J. S.; Saito, R.; *et al.* Raman and Fluorescence Spectroscopic Studies of a DNA-Dispersed Double-Walled Carbon Nanotube Solution. *ACS Nano* **2010**, *4*, 1060–1066.
80. Green, A. A.; Hersam, M. C. Processing and Properties of Highly Enriched Double-Wall Carbon Nanotubes. *Nat. Nanotechnol.* **2009**, *4*, 64–70.
81. Tsyboulski, D. A.; Hou, Y.; Fakhri, N.; Ghosh, S.; Zhang, R.; Bachilo, S. M.; Pasquali, M.; Chen, L.; Liu, J.; Weisman, R. B. Do Inner Shells of Double-Walled Carbon Nanotubes Fluoresce? *Nano Lett.* **2009**, *9*, 3282–3289.
82. Fantini, C.; Jorio, A.; Souza, M.; Strano, M. S.; Dresselhaus, M. S.; Pimenta, M. A. Optical Transition Energies for Carbon Nanotubes from Resonant Raman Spectroscopy: Environment and Temperature Effects. *Phys. Rev. Lett.* **2004**, *93*, 147406.
83. Telg, H.; Maultzsch, J.; Reich, S.; Hennrich, F.; Thomsen, C. Chirality Distribution and Transition Energies of Carbon Nanotubes. *Phys. Rev. Lett.* **2004**, *93*, 177401.
84. Meyer, J. C.; Paillet, M.; Michel, T.; Moreac, A.; Neumann, A.; Duesberg, G. S.; Roth, S.; Sauvajol, J. L. Raman Modes of Index-Identified Freestanding Single-Walled Carbon Nanotubes. *Phys. Rev. Lett.* **2005**, *95*, 217401.
85. Kataura, H.; Kumazawa, Y.; Maniwa, Y.; Umezu, I.; Suzuki, S.; Ohtsuka, Y.; Achiba, Y. Optical Properties of Single-Wall Carbon Nanotubes. *Synth. Met.* **1999**, *103*, 2555–2558.
86. Paillet, M.; Michel, T.; Meyer, J. C.; Popov, V. N.; Henrard, L.; Roth, S.; Sauvajol, J. L. Raman Active Phonons of Identified Semiconducting Single-Walled Carbon Nanotubes. *Phys. Rev. Lett.* **2006**, *96*, 257401.
87. Jorio, A.; Saito, R.; Hafner, J. H.; Lieber, C. M.; Hunter, M.; McClure, T.; Dresselhaus, G.; Dresselhaus, M. S. Structural (*n*,*m*) Determination of Isolated Single-Wall Carbon Nanotubes by Resonant Raman Scattering. *Phys. Rev. Lett.* **2001**, *86*, 1118–1121.
88. Araujo, P. T.; Doorn, S. K.; Kilina, S.; Tretiak, S.; Einarsson, E.; Maruyama, S.; Chacham, H.; Pimenta, M. A.; Jorio, A. Third and Fourth Optical Transitions in Semiconducting Carbon Nanotubes. *Phys. Rev. Lett.* **2007**, *98*, 067401.
89. Villalpando-Paez, F.; Moura, L. G.; Fantini, C.; Muramatsu, H.; Hayashi, T.; Kim, Y. A.; Endo, M.; Terrones, M.; Pimenta, M. A.; Dresselhaus, M. S. Tunable Raman Spectroscopy Study of CVD and Peapod-Derived Bundled and Individual Double-Wall Carbon Nanotubes. *Phys. Rev. B* **2010**, *82*, 155416.
90. Lazzeri, M.; Piscanec, S.; Mauri, F.; Ferrari, A. C.; Robertson, J. Phonon Linewidths and Electron—Phonon Coupling in Graphite and Nanotubes. *Phys. Rev. B* **2006**, *73*, 155426.
91. Piscanec, S.; Lazzeri, M.; Robertson, J.; Ferrari, A. C.; Mauri, F. Optical Phonons in Carbon Nanotubes: Kohn Anomalies, Peierls Distortions, and Dynamic Effects. *Phys. Rev. B* **2007**, *75*, 035427.
92. Ferrari, A. C.; Meyer, J. C.; Scardaci, V.; Casiraghi, C.; Lazzeri, M.; Mauri, F.; Piscanec, S.; Jiang, D.; Novoselov, K. S.; Roth, S.; *et al.* Raman Spectrum of Graphene and Graphene Layers. *Phys. Rev. Lett.* **2006**, *97*, 187401.
93. Jorio, A.; Santos, A. P.; Ribeiro, H. B.; Fantini, C.; Souza, M.; Vieira, J. P. M.; Furtado, C. A.; Jiang, J.; Saito, R.; Balzano, L.; *et al.* Quantifying Carbon-Nanotube Species with Resonance Raman Scattering. *Phys. Rev. B* **2005**, *72*, 075207.
94. Barros, E. B.; Son, H.; Samsonidze, G. G.; Souza Filho, A. G.; Saito, R.; Kim, Y. A.; Muramatsu, H.; Hayashi, T.; Endo, M.; Kong, J.; *et al.* Raman Spectroscopy of Double-Walled Carbon Nanotubes Treated with $H_2SO_4$. *Phys. Rev. B* **2007**, *76*, 045425.
95. Cançado, L. G.; Jorio, A.; Ferreira, E. H. M.; Stavale, F.; Achete, C. A.; Capaz, R. B.; Moutinho, M. V. O.; Lombardo, A.; Kulmala, T. S.; Ferrari, A. C. Quantifying Defects in Graphene *via* Raman Spectroscopy at Different Excitation Energies. *Nano Lett.* **2011**, *11*, 3190–3196.

96. Tuinstra, F.; Koenig, J. L. Raman Spectrum of Graphite. *J. Chem. Phys.* **1970**, *53*, 1126–1130.
97. Ren, W.; Li, F.; Tan, P.; Cheng, H.-M. Raman Evidence for Atomic Correlation between the Two Constituent Tubes in Double-Walled Carbon Nanotubes. *Phys. Rev. B* **2006**, *73*, 115430.
98. Bonaccorso, F.; Hasan, T.; Tan, P. H.; Sciascia, C.; Privitera, G.; Di Marco, G.; Gucciardi, P. G.; Ferrari, A. C. Density Gradient Ultracentrifugation of Nanotubes: Interplay of Bundling and Surfactants Encapsulation. *J. Phys. Chem. C* **2010**, *114*, 17267–17285.
99. Hasan, T.; Scardaci, V.; Tan, P. H.; Rozhin, A. G.; Milne, W. I.; Ferrari, A. C. Stabilization and "Debundling" of Single-Wall Carbon Nanotube Dispersions in *N*-Methyl-2-pyrrolidone (NMP) by Polyvinylpyrrolidone (PVP). *J. Phys. Chem. C* **2007**, *111*, 12594–12602.
100. Hasan, T.; Tan, P. H.; Bonaccorso, F.; Rozhin, A.; Scardaci, V.; Milne, W.; Ferrari, A. C. Polymer-Assisted Isolation of Single Wall Carbon Nanotubes in Organic Solvents for Optical-Quality Nanotube−Polymer Composites. *J. Phys. Chem. C* **2008**, *112*, 20227–20232.
101. Cheng, Q. H.; Debnath, S.; Gregan, E.; Byrne, H. J. Effect of Solvent Solubility Parameters on the Dispersion of Single-Walled Carbon Nanotubes. *J. Phys. Chem. C* **2008**, *112*, 20154–20158.
102. Travers, J. C.; Morgenweg, J.; Obraztsova, E. D.; Chernov, A. I.; Kelleher, E. J. R.; Popov, S. V. Using the $E_{22}$ Transition of Carbon Nanotubes for Fiber Laser Mode-Locking. *Laser Phys. Lett.* **2011**, *8*, 144–149.
103. Manzoni, C.; Gambetta, A.; Menna, E.; Meneghetti, M.; Lanzani, G.; Cerullo, G. Intersubband Exciton Relaxation Dynamics in Single-Walled Carbon Nanotubes. *Phys. Rev. Lett.* **2005**, *94*, 207401.
104. Reich, S.; Dworzac, M.; Hoffmann, A.; Thomsen, C.; Strano, M. S. Excited-State Carrier Lifetime in Single-Walled Carbon Nanotubes. *Phys. Rev. B* **2005**, *71*, 03340.
105. Cho, W. B.; Yim, J. H.; Choi, S. Y.; Lee, S.; Schmidt, A.; Steinmeyer, G.; Griebner, U.; Petrov, V.; Yeom, D.-I.; Kim, K.; *et al.* Boosting the Non Linear Optical Response of Carbon Nanotube Saturable Absorbers for Broadband Mode-Locking of Bulk Lasers. *Adv. Funct. Mater.* **2010**, *20*, 1937–1943.
106. Bohren, C. F.; Huffman, D. R. *Absorption and Scattering of Light by Small Particles*; Wiley-Interscience: New York, 1998.
107. Agrawal, G. P. *Nonlinear Fiber Optics*; Academic Press: New York, 2001.
108. Dennis, M. L.; Duling, I. N. Experimental Study of Sideband Generation in Femtosecond Fiber Lasers. *IEEE J. Quantum Electron.* **1994**, *30*, 1469–1477.
109. Pandit, N.; Noske, D. U.; Kelly, S. M. J.; Taylor, J. R. Characterstic Instability of Fibre Loop Soliton Lasers. *Electron. Lett.* **1992**, *28*, 455–457.
110. Von der Linde, D. Characterization of the Noise in Continuously Operating Mode-Locked Lasers. *Appl. Phys. B: Laser Opt.* **1986**, *39*, 201–217.
111. Keller, U. In *Progress in Optics*; Wolf, E., Ed.; Elsevier: Amsterdam, 2004; Vol. 46.